J. Fluid Mech. (2001), *vol.* 444, *pp.* 1–21. Printed in the United Kingdom

Acoustic radiation interparticle forces in a compressible fluid

By ALEXANDER A. DOINIKOV

Institute of Nuclear Problems, Byelorussian State University, Belarus

(Received 23 March 2000 and in revised form 13 March 2001)

An analytical expression is derived for the time-averaged radiation force induced by an acoustic wave field between N particles freely suspended in a fluid. Both the host fluid and the medium inside the particles are assumed to be ideal compressible fluids. The incident field is assumed to be moderate so that the scattered and refracted fields of the particles can be taken to linear approximation. Multiple re-scattering of sound between the particles and shape modes of all orders are allowed for. No restrictions are imposed on the size of the particles, the separation distances between them and their number. The present study substantially extends the existing theory, which is based on essential simplifications and valid only for pairwise interactions. In particular, the new theory allows one to follow continuously the evolution of the radiation interaction force from large to small separation distances. The general results are illustrated in the case of two air bubbles in water. It is shown that generally the interbubble force behaves in far more complicated way than is predicted by the classical Bjerknes theory.

1. Introduction

The intrinsically nonlinear nature of wave motion in fluids results in a great variety of nonlinear effects. One such effect is the time-averaged radiation interaction forces that are induced by an acoustic wave field between foreign inclusions (bubbles, drops, etc.) suspended in a fluid. Interest in this phenomenon is motivated by a number of important applications, such as acoustic cavitation, acoustic coagulation and precipitation of aerosols, biomedical ultrasonics, etc. (Brennen 1995; Mednikov 1965; Rozenberg 1973). The existing theory of acoustic interaction forces is based on an investigation of pairwise interactions between particles, even though the ultimate aim is simulation of multi-particle structures. Most of the theoretical work deals with bubble–bubble interactions; for reviews see Crum (1975), Pelekasis & Tsamopoulos (1993*a*, *b*), Doinikov & Zavtrak (1995, 1997), and Mettin *et al.* (1997). There are also papers on the interaction forces between particles of different nature (König 1891; Embleton 1962; Mednikov 1965; Weiser & Apfel 1984; Doinikov & Zavtrak 1996; Doinikov 1996).

Because of mathematical difficulties, early investigators substantially simplified the problem. They started from the following basic assumptions: (*a*) the surrounding medium is an ideal incompressible fluid; (*b*) the spacing between objects is much larger than their size; (*c*) the gas within bubbles obeys the adiabatic law, and liquid drops can be treated as rigid spheres; (*d*) nonlinear oscillations of the interacting objects are negligible. Subsequent studies have attempted to improve the theory, examining what happens to the interaction force when one of the above assumptions is discarded

while the others remain the same. In particular, investigations of the interaction forces at small separation distances for various pairs of particles (bubble–bubble, bubble–solid, bubble–drop, solid–solid) have been carried out (Zabolotskaya 1984; Doinikov & Zavtrak 1995, 1996; Doinikov 1996). Their results give an explanation for stable bubble clusters, 'bubble grapes', which were observed experimentally by Kobelev, Ostrovskii & Sutin (1979), and also predict a number of new interesting effects. For the case of two bubbles, the situation has also been considered where the separation distance, remaining large compared with the bubble radii, is comparable with or more than the wavelength of sound (Zheng & Apfel 1995; Doinikov & Zavtrak 1997). Under such conditions, the calculation of the interaction force requires allowing for the compressibility of the host fluid. This, apart from a modification of the original force, results in two additional long-range components inversely proportional to the separation distance instead of the distance squared, one of these acting along the centreline of the bubbles and the other along the gradient of the imposed acoustic field. Moreover, the sign of the combined force becomes dependent on the separation distance, which can give rise to bound bubble pairs with some stable spacing.

The present state of the art in mathematics makes it possible to develop a more general theory that would allow for the compressibility of the host fluid and the internal medium of particles, multiple rescattering of sound between the particles and their shape modes, while at the same time being free of any restrictions on the size of the particles, the spacing between them, the wavelength of sound outside and inside the particles, and moreover valid for an arbitrary number of particles. The only limitations would be the assumptions that the media outside and inside particles are inviscid and the forcing is relatively weak. This approach could recover, integrate and substantially extend all the currently available analytical results. In particular, specifying appropriately the parameters of the host fluid and the media inside interacting objects, we would be able to obtain the interaction force between various pairs of objects (bubble–bubble, bubble–drop, drop–drop) for arbitrary separation distances and angles of sound incidence, which would allow us to follow continuously the evolution of the interaction force from large to small separation distances. It is the purpose of the present research to develop such a theory.

2. Theory

Let N particles (bubbles or drops, or both) be freely suspended in a fluid irradiated by an acoustic wave field. Assume that (*a*) the media outside and inside the particles are ideal compressible fluids subject to the Euler equation; (*b*) the particles are spherical at rest; (*c*) the incident field is moderate so that the scattered and refracted fields of the particles can be taken in linear approximation; (*d*) sufficiently long time has elapsed since the sound was turned on so that free oscillations of the particles and associated transient processes have died out and the particles now oscillate with the driving frequency alone. The purpose of the research is to derive an analytical expression, accurate to the second order in the acoustic pressure amplitude, for the time-averaged interaction force induced by the incident acoustic field between the particles, provided that no restrictions are imposed on the radii of the particles, the separations between them and the wavelength of sound outside and inside the particles, and that shape modes of all orders and multiple re-scattering of sound between the particles are allowed for. It is pertinent to recall here that an inviscid fluid has a useful feature as regards the acoustic radiation force. Namely, though this force is a nonlinear effect, quadratic in the acoustic pressure amplitude, its calculation

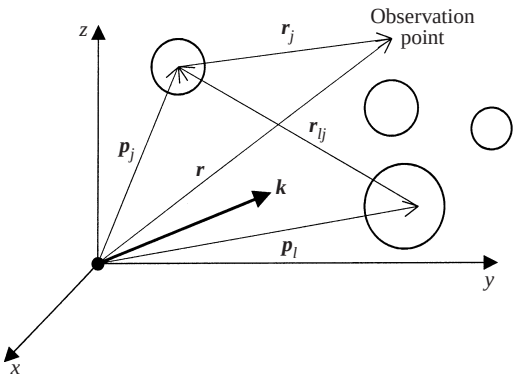

FIGURE 1. Geometry of the system.

in the context of inviscid fluid behaviour only requires knowledge of the linear scattered field of the particles. This feature, which significantly facilitates the task, is used in the present study.

The geometry of the system to be investigated is shown in figure 1. The motion of the particles is observed with reference to the global Cartesian coordinates (x, y, z) with the unit vectors $\boldsymbol{e}_x, \boldsymbol{e}_y, \boldsymbol{e}_z$. Each particle has also its own local spherical coordinate system $(r_j, \theta_j, \varepsilon_j)$, $j = 1, 2, \ldots N$, the origin of which is at its equilibrium centre.

2.1. *Incident field*

The velocity potential of the incident field is taken in the following general form:

$$\varphi_{inc}^{(j)}(\boldsymbol{r}_j, t) = \mathrm{e}^{-\mathrm{i}\omega t} \sum_{n=0}^{\infty} \sum_{m=-n}^{n} A_{nm}^{(j)} j_n(kr_j) Y_{nm}(\theta_j, \varepsilon_j), \tag{2.1}$$

where the index (j) implies that (2.1) gives the incident field in the vicinity of the jth particle, t is time, ω the angular driving frequency, k the wavenumber in the host fluid, j_n the spherical Bessel function, and Y_{nm} the spherical harmonics. The multipole coefficients $A_{nm}^{(j)}$, which are responsible for a specific type of incident field, are assumed here to be known. Explicit expressions for these coefficients in the cases of a plane travelling wave and a plane standing wave are given in § 2.4. The spherical harmonics Y_{nm} are defined as

$$Y_{nm}(\theta, \varepsilon) = \left[\frac{(2n+1)(n-m)!}{4\pi(n+m)!}\right]^{1/2} P_n^m(\cos\theta)\mathrm{e}^{\mathrm{i}m\varepsilon}, \quad Y_{n(-m)}(\theta, \varepsilon) = (-1)^m Y_{nm}(\theta, -\varepsilon), \tag{2.2}$$

where $P_n^m(x)$ denotes the associated Legendre polynomials given by (Abramowitz & Stegun 1972)

$$P_n^m(x) = (-1)^m (1-x^2)^{m/2} \frac{\mathrm{d}^m P_n(x)}{\mathrm{d}x^m}, \quad m \geqslant 0. \tag{2.3}$$

2.2. *Scattered and refracted fields*

The general expressions for the scattered (outside) field and the refracted (inside) field of the jth particle, satisfying the linear equations of motion of an ideal compressible fluid, can be written as

$$\varphi_{sca}^{(j)}(\boldsymbol{r}_j, t) = \mathrm{e}^{-\mathrm{i}\omega t} \sum_{n=0}^{\infty} \sum_{m=-n}^{n} B_{nm}^{(j)} h_n^{(1)}(kr_j) Y_{nm}(\theta_j, \varepsilon_j), \tag{2.4}$$

$$\varphi_{ref}^{(j)}(\boldsymbol{r}_j, t) = \mathrm{e}^{-\mathrm{i}\omega t} \sum_{n=0}^{\infty} \sum_{m=-n}^{n} C_{nm}^{(j)} j_n(k_j r_j) Y_{nm}(\theta_j, \varepsilon_j), \tag{2.5}$$

where $B_{nm}^{(j)}$ and $C_{nm}^{(j)}$ are, respectively, the scattering and refraction coefficients to be determined by the boundary conditions at the surface of the jth particle, $h_n^{(1)}$ is the spherical Hankel function of the first kind, and k_j is the wavenumber inside the jth particle. Since we are to calculate the force on the jth particle, we must know multipole expansions for the scattered fields of all the other particles in terms of the spherical coordinates attached to the jth particle. This can be achieved by using the so-called addition theorems for spherical wave functions, see Koc & Chew (1998). As a result, the scattered field of the lth particle near the surface of the jth particle can be represented as

$$\varphi_{sca}^{(lj)}(\boldsymbol{r}_j, t) = \mathrm{e}^{-\mathrm{i}\omega t} \sum_{n=0}^{\infty} \sum_{m=-n}^{n} B_{nm}^{(lj)} j_n(k r_j) Y_{nm}(\theta_j, \varepsilon_j), \tag{2.6}$$

where the coefficients $B_{nm}^{(lj)}$ are given by

$$B_{nm}^{(lj)} = \sum_{\nu=0}^{\infty} \sum_{\mu=-\nu}^{\nu} B_{\nu\mu}^{(l)} K_{nm\nu\mu}(k, \boldsymbol{r}_{lj}), \tag{2.7}$$

the vector $\boldsymbol{r}_{lj} = \boldsymbol{p}_j - \boldsymbol{p}_l$ is drawn from the equilibrium centre of the lth particle to that of the jth particle, and $\boldsymbol{p}_j$ is the position vector of the jth particle with respect to the global coordinates, see figure 1. The connection coefficients $K_{nm\nu\mu}$ are specified by

$$K_{nm\nu\mu}(k, \boldsymbol{r}) = (-1)^m \mathrm{i}^{n-\nu} [4\pi(2n+1)(2\nu+1)]^{1/2} \sum_{\nu'=|n-\nu|}^{n+\nu} \mathrm{i}^{\nu'} h_{\nu'}^{(1)}(kr) Y_{\nu'\mu-m}(\theta, \varepsilon)$$
$$\times (2\nu'+1)^{-1/2} (\nu n 00 | \nu n \nu' 0)(\nu n \mu' m | \nu n \nu' \mu''), \tag{2.8}$$

where $\mu' = -\mu$, $\mu'' = m - \mu$, and $(j_1 j_2 m_1 m_2 | j_1 j_2 j m)$ denotes the Clebsch–Gordan coefficients as defined in Abramowitz & Stegun (1972).

The total acoustic field in the vicinity of the jth particle can now be written as

$$\Phi_j(\boldsymbol{r}_j, t) = \varphi_{inc}^{(j)} + \varphi_{sca}^{(j)} + \sum_{\substack{l=1 \\ l \neq j}}^{N} \varphi_{sca}^{(lj)}. \tag{2.9}$$

To obtain the unknown coefficients $B_{nm}^{(j)}$ and $C_{nm}^{(j)}$, the boundary conditions at the surface $S_j(t)$ of the jth particle are applied. To linear approximation this surface can be represented as (Lamb 1945)

$$S_j(t): \quad f_j(\boldsymbol{r}_j, t) \equiv r_j - R_j - \mathrm{e}^{-\mathrm{i}\omega t} \sum_{n=0}^{\infty} \sum_{m=-n}^{n} a_{nm}^{(j)} Y_{nm}(\theta_j, \varepsilon_j) = 0, \tag{2.10}$$

where R_j is the equilibrium radius of the jth particle and the amplitudes of the surface modes $a_{nm}^{(j)}$ are yet to be determined. It is assumed that $|a_{nm}^{(j)}| \ll R_j$ since the forcing is weak. Combining the kinematical boundary condition,

$$\frac{\partial f_j}{\partial t} + \nabla \Phi_j \cdot \nabla f_j = 0 \quad \text{at} \quad r_j = R_j, \tag{2.11}$$

with the boundary condition for the normal velocities on the outer and inner sides of $S_j(t)$,

$$\frac{\partial \Phi_j}{\partial r_j} = \frac{\partial \varphi_{ref}^{(j)}}{\partial r_j} \quad \text{at} \quad r_j = R_j, \tag{2.12}$$

one obtains

$$\frac{\partial \varphi_{ref}^{(j)}}{\partial r_j} = -\frac{\partial f_j}{\partial t} \quad \text{at} \quad r_j = R_j. \tag{2.13}$$

Substituting (2.5) and (2.10), one expresses $a_{nm}^{(j)}$ in terms of the refraction coefficients

$$a_{nm}^{(j)} = \frac{\mathrm{i}k_j}{\omega} j_n'(k_j R_j) C_{nm}^{(j)}, \tag{2.14}$$

where the prime denotes differentiation with respect to the argument in parentheses. Upon substitution of (2.1), (2.4)–(2.6) and (2.9), (2.12) also yields an equation connecting the scattering and refraction coefficients

$$A_{nm}^{(j)} j_n'(x_j) + B_{nm}^{(j)} h_n^{(1)'}(x_j) + \sum_{\substack{l=1 \\ l \neq j}}^{N} B_{nm}^{(lj)} j_n'(x_j) = C_{nm}^{(j)} y_j j_n'(y_j)/x_j, \tag{2.15}$$

where $x_j = kR_j$ and $y_j = k_j R_j$.

Another equation is provided by the boundary condition for normal stresses

$$P_0 + P_{\sigma j} - \rho_0 \frac{\partial \Phi_j}{\partial t} = P_{j0} - \rho_j \frac{\partial \varphi_{ref}^{(j)}}{\partial t} \quad \text{at} \quad r_j = R_j, \tag{2.16}$$

where P_0, ρ_0 are the equilibrium pressure and density of the host fluid, P_{j0}, ρ_j are the equilibrium pressure and density inside the jth particle, and $P_{\sigma j}$ is the pressure of surface tension, given by (Prosperetti 1977)

$$P_{\sigma j}(\theta_j, \varepsilon_j, t) = \sigma_j \Delta f_j|_{S_j} = \frac{2\sigma_j}{R_j} + \frac{\sigma_j}{R_j^2} \mathrm{e}^{-\mathrm{i}\omega t} \sum_{n=0}^{\infty} \sum_{m=-n}^{n} (n-1)(n+2) a_{nm}^{(j)} Y_{nm}(\theta_j, \varepsilon_j), \tag{2.17}$$

σ_j being the surface tension coefficient at the interface of the host fluid and the jth particle. Substituting (2.1), (2.4)–(2.6), (2.9) and (2.17) into (2.16) and using (2.14), one obtains the trivial relation $P_{j0} = P_0 + 2\sigma_j/R_j$ and the second equation connecting the scattering and refraction coefficients,

$$A_{nm}^{(j)} j_n(x_j) + B_{nm}^{(j)} h_n^{(1)}(x_j) + \sum_{\substack{l=1 \\ l \neq j}}^{N} B_{nm}^{(lj)} j_n(x_j) = \alpha_n^{(j)} C_{nm}^{(j)}, \tag{2.18}$$

where

$$\alpha_n^{(j)} = \frac{\rho_j}{\rho_0} j_n(y_j) - \frac{y_j \sigma_j (n-1)(n+2)}{\rho_0 R_j^3 \omega^2} j_n'(y_j). \tag{2.19}$$

Combining (2.15) and (2.18), one can express the refraction coefficients in terms of the scattering coefficients

$$C_{nm}^{(j)} = \beta_n^{(j)} B_{nm}^{(j)}, \tag{2.20}$$

where

$$\beta_n^{(j)} = \frac{x_j}{\mathrm{Re}\{H_n^{(j)}\}}[j_n(x_j)h_n^{(1)'}(x_j) - j_n'(x_j)h_n^{(1)}(x_j)], \tag{2.21}$$

$$H_n^{(j)} = y_j j_n'(y_j)h_n^{(1)}(x_j) - x_j\alpha_n^{(j)}h_n^{(1)'}(x_j), \tag{2.22}$$

and Re means 'the real part of'. Eliminating $B_{nm}^{(lj)}$ and $C_{nm}^{(j)}$ from (2.15) and (2.18) with the aid of (2.7) and (2.20), one finds

$$B_{nm}^{(j)} + Q_n^{(j)} + \sum_{\substack{l=1\\ l\neq j}}^{N}\sum_{\nu=0}^{\infty}\sum_{\mu=-\nu}^{\nu} K_{nm\nu\mu}(k, \boldsymbol{r}_{lj})B_{\nu\mu}^{(l)} = -Q_n^{(j)}A_{nm}^{(j)}, \tag{2.23}$$

where

$$Q_n^{(j)} = \mathrm{Re}\{H_n^{(j)}\}/H_n^{(j)}. \tag{2.24}$$

Equation (2.23) provides us with a set of equations for calculating the unknown scattering coefficients. This set is four-dimensional. The first, 'horizontal', dimension is given by the index ν. The second, 'vertical', dimension is set by the index n. These two indices are determined by the number of terms that are retained in the multipole expansions of the incident, scattered, and refracted fields. The third, 'spatial', dimension is established by the index m (and μ), which ranges from $-n$ to n. In the case of two particles, non-vanishing coefficients with non-zero m appear if the wavevector is not aligned with the centreline of the particles. Needless to say that, in the case of many particles, such coefficients are always present. The fourth, 'particle', dimension is assigned by the superscript j (and l), which is responsible for the number of particles in the system. It is obvious that in the general case the set of equations (2.23) can be solved only numerically, setting the index n (and hence ν) to a limiting value. As noted above, physically this means that we restrict our analysis to a finite number of the multipole contributions.

2.3. *Calculation of the force*

The general formula for the acoustic radiation force on an arbitrary object in an ideal compressible fluid is given by (Alekseev 1983)

$$\boldsymbol{F} = \rho_0 \int_{S_0} \left\langle \frac{1}{2}v^2\boldsymbol{n} - \frac{1}{2c^2}\left(\frac{\partial\Phi}{\partial t}\right)^2\boldsymbol{n} - \boldsymbol{v}(\boldsymbol{v}\cdot\boldsymbol{n})\right\rangle \mathrm{d}S_0. \tag{2.25}$$

where S_0 is the unperturbed surface of the object, $\boldsymbol{n}$ the outward normal to S_0, c the speed of sound in the host fluid, $\boldsymbol{v} = \nabla\Phi$ the fluid velocity, and $\langle\ \rangle$ denotes an average over time. Applying this formula to our case and substituting in it all the required quantities from the preceding subsection, the force on the jth particle can be represented as

$$\boldsymbol{F}_j = -\frac{\rho_0}{4}\mathrm{Re}\sum_{n=0}^{\infty}\sum_{n'=0}^{\infty}\sum_{m=-n}^{n}\sum_{m'=-n'}^{n'} C_{nm}^{(j)}C_{n'm'}^{(j)*}\{[x_j^2\alpha_n^{(j)}\alpha_{n'}^{(j)} + y_j^2 j_n'(y_j)j_{n'}'(y_j)]$$
$$\times\boldsymbol{I}_1(n,m,n',m') + 2y_j\alpha_n^{(j)}j_{n'}'(y_j)\boldsymbol{I}_2(n,m,n',m') - \alpha_n^{(j)}\alpha_{n'}^{(j)}\boldsymbol{I}_3(n,m,n',m')\}, \tag{2.26}$$

where

$$\boldsymbol{I}_1(n,m,n',m') = \int_0^{2\pi}\mathrm{d}\varepsilon\int_0^{\pi}\mathrm{d}\theta\sin\theta\, Y_{nm}(\theta,\varepsilon)Y_{n'm'}^*(\theta,\varepsilon)\boldsymbol{e}_r, \tag{2.27}$$

$$\boldsymbol{I}_2(n,m,n',m') = \int_0^{2\pi} \mathrm{d}\varepsilon \int_0^{\pi} \mathrm{d}\theta \sin\theta \, Y^*_{n'm'}(\theta,\varepsilon)\nabla_t Y_{nm}(\theta,\varepsilon), \tag{2.28}$$

$$\boldsymbol{I}_3(n,m,n',m') = \int_0^{2\pi} \mathrm{d}\varepsilon \int_0^{\pi} \mathrm{d}\theta \sin\theta [\nabla_t Y_{nm}(\theta,\varepsilon) \cdot \nabla_t Y^*_{n'm'}(\theta,\varepsilon)]\boldsymbol{e}_r, \tag{2.29}$$

the asterisk denotes the complex conjugate, and the operator ∇_t is defined as

$$\nabla_t = \boldsymbol{e}_\theta \frac{\partial}{\partial\theta} + \frac{\boldsymbol{e}_\varepsilon}{\sin\theta}\frac{\partial}{\partial\varepsilon}. \tag{2.30}$$

Values of integrals (2.27)–(2.29) and an explanation of how they are calculated are given in the Appendix. Substituting them into (2.26) and using (2.20), one obtains the final expression for the acoustic radiation force on the jth particle:

$$\begin{aligned}\boldsymbol{F}_j = \rho_0 \,\mathrm{Re} \sum_{n=0}^{\infty}\sum_{m=-n}^{n} D_n^{(j)} B_{nm}^{(j)} \Big\{ & 2\sqrt{(n+1)^2-m^2}\, B^{(j)*}_{(n+1)m}\boldsymbol{e}_z \\ & + \sqrt{(n-m+1)(n-m+2)}\, B^{(j)*}_{(n+1)(m-1)}(\boldsymbol{e}_x + \mathrm{i}\boldsymbol{e}_y) \\ & - \sqrt{(n+m+1)(n+m+2)}\, B^{(j)*}_{(n+1)(m+1)}(\boldsymbol{e}_x - \mathrm{i}\boldsymbol{e}_y)\Big\},\end{aligned} \tag{2.31}$$

where

$$\begin{aligned}D_n^{(j)} = \frac{\beta_n^{(j)}\beta_{n+1}^{(j)*}}{4\sqrt{(2n+1)(2n+3)}} \{ & [n(n+2)-x_j^2]\alpha_n^{(j)}\alpha_{n+1}^{(j)} + n y_j \alpha_n^{(j)} j'_{n+1}(y_j) \\ & - (n+2) y_j \alpha_{n+1}^{(j)} j'_n(y_j) - y_j^2 j'_n(y_j) j'_{n+1}(y_j)\}.\end{aligned} \tag{2.32}$$

Note that (2.31) involves both the primary and the secondary radiation forces. This equation also shows that the force is expressed in terms of the liner scattering coefficients $B_{nm}^{(j)}$ multiplied by the known functions $D_n^{(j)}$. Therefore the main point in calculating the force is the calculation of the coefficients $B_{nm}^{(j)}$ from the set of equations (2.23). If they are known, then the force can easily be found from (2.31) for any values of the system parameters.

2.4. *Examples of explicit expressions for the coefficients* $A_{nm}^{(j)}$

In this subsection, it is shown how the coefficients $A_{nm}^{(j)}$ are found, which specify the incident field in the vicinity of the jth particle. By way of example let us consider two types of forcing – a plane travelling wave and a plane standing wave.

2.4.1. *Plane travelling wave*

In terms of the global coordinates (figure 1), the velocity potential of a plane travelling wave can be represented as

$$\varphi_{inc}(\boldsymbol{r},t) = A\exp(\mathrm{i}\boldsymbol{k}\cdot\boldsymbol{r} - \mathrm{i}\omega t), \tag{2.33}$$

where $\boldsymbol{k}$ is the wavevector in the host fluid. Taking into consideration that $\boldsymbol{r} = \boldsymbol{p}_j + \boldsymbol{r}_j$, (2.33) can be rewritten in terms of the coordinates related to the jth particle as

$$\varphi_{inc}^{(j)}(\boldsymbol{r}_j,t) = A\exp(\mathrm{i}\boldsymbol{k}\cdot\boldsymbol{p}_j - \mathrm{i}\omega t)\exp(\mathrm{i}\boldsymbol{k}\cdot\boldsymbol{r}_j). \tag{2.34}$$

By using the well-known multipole expansion for exponential function (Abramowitz & Stegun 1972), one obtains

$$\varphi_{inc}^{(j)}(\boldsymbol{r}_j,t) = 4\pi A\exp(\mathrm{i}\boldsymbol{k}\cdot\boldsymbol{p}_j)\mathrm{e}^{-\mathrm{i}\omega t}\sum_{n=0}^{\infty}\sum_{m=-n}^{n} \mathrm{i}^n Y^*_{nm}(\theta_I,\varepsilon_I) j_n(kr_j) Y_{nm}(\theta_j,\varepsilon_j), \tag{2.35}$$

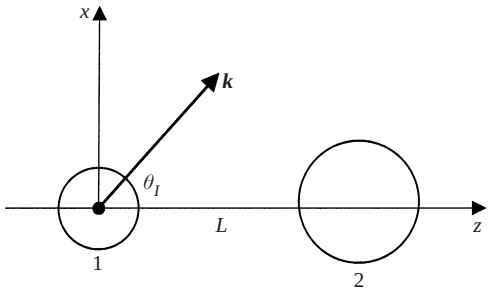

FIGURE 2. Case of two particles.

where θ_I, ε_I are the angles that specify the direction of the wavevector $\boldsymbol{k}$ in the global coordinates. Comparisons of (2.35) with (2.1) finally yields

$$A_{nm}^{(j)} = 4\pi A \exp(\mathrm{i}\boldsymbol{k}\cdot p_j)\mathrm{i}^n Y_{nm}^*(\theta_I, \varepsilon_I). \tag{2.36}$$

2.4.2. *Plane standing wave*

The velocity potential of a plane standing wave can be written as

$$\varphi_{inc}(\boldsymbol{r}, t) = A\exp(-\mathrm{i}\omega t)\cos(\boldsymbol{k}\cdot\boldsymbol{r} + kd_o), \tag{2.37}$$

where d_o is the distance between the origin of the coordinate system shown in figure 1 and the nearest velocity node plane of the incident standing wave. In terms of the coordinates related to the jth particle, (2.37) can be rewritten as

$$\varphi_{inc}^{(j)}(\boldsymbol{r}_j, t) = A\exp(-\mathrm{i}\omega t)\cos(\boldsymbol{k}\cdot\boldsymbol{r}_j + kd_j) = \tfrac{1}{2}A\exp(-\mathrm{i}\omega t)[\exp(\mathrm{i}kd_j)\exp(\mathrm{i}\boldsymbol{k}\cdot\boldsymbol{r}_j) + \text{c.c.}], \tag{2.38}$$

where d_j is now the distance between the velocity node plane and the equilibrium centre of the jth particle. Using again the multipole expansion for the function $\exp(\mathrm{i}\boldsymbol{k}\cdot\boldsymbol{r}_j)$ and comparing the resulting expression with (2.1), one finds

$$A_{nm}^{(j)} = 2\pi A\mathrm{i}^n Y_{nm}^*(\theta_I, \varepsilon_I)[\exp(\mathrm{i}kd_j) + (-1)^n\exp(-\mathrm{i}kd_j)]. \tag{2.39}$$

2.5. *Case of two-particle interaction*

In the case of two particles, the set of equations (2.23) reduces to

$$B_{nm}^{(1)} + Q_n^{(1)}\sum_{\nu=0}^{\infty}\sum_{\mu=-\nu}^{\nu} K_{nm\nu\mu}(k, \boldsymbol{r}_{21})B_{\nu\mu}^{(2)} = -Q_n^{(1)}A_{nm}^{(1)}, \tag{2.40}$$

$$B_{nm}^{(2)} + Q_n^{(2)}\sum_{\nu=0}^{\infty}\sum_{\mu=-\nu}^{\nu} K_{nm\nu\mu}(k, \boldsymbol{r}_{12})B_{\nu\mu}^{(1)} = -Q_n^{(2)}A_{nm}^{(2)}. \tag{2.41}$$

Choosing the global coordinate system as shown in figure 2 and denoting by L the distance between the equilibrium centres of the particles, one has $\boldsymbol{r}_{12} = L\boldsymbol{e}_z$, $r_{21} = -L\boldsymbol{e}_z$ and hence $\theta_{12} = 0$, $\theta_{21} = \pi$, $\varepsilon_{12} = \varepsilon_{21} = 0$. Using the properties of spherical harmonics (Varshalovich, Moskalev & Khersonskii 1975)

$$Y_{nm}(0, \varepsilon) = \delta_{m0}\sqrt{(2n+1)/4\pi}, \quad Y_{nm}(\pi, \varepsilon) = \delta_{m0}(-1)^n\sqrt{(2n+1)/4\pi}, \tag{2.42}$$

where δ_{m0} is the Kronecker delta, (2.40) and (2.41) can be simplified to

$$B_{nm}^{(1)} + Q_n^{(1)} \sum_{v=|m|}^{\infty} K_{nmv}^{(1)} B_{vm}^{(2)} = -Q_n^{(1)} A_{nm}^{(1)}, \tag{2.43}$$

$$B_{nm}^{(2)} + Q_n^{(2)} \sum_{v=|m|}^{\infty} K_{nmv}^{(2)} B_{vm}^{(1)} = -Q_n^{(2)} A_{nm}^{(2)}, \tag{2.44}$$

where

$$K_{nmv}^{(j)} = (-1)^m \mathrm{i}^{n-v} \sqrt{(2n+1)(2v+1)} \sum_{l=|n-v|}^{n+v} (-1)^{jl} i^l h_l^{(1)}(kL) \times (vn00|vnl0)(vn-mm|vnl0), \quad j = 1, 2. \tag{2.45}$$

Eliminating $B_{nm}^{(2)}$ from the equation for $B_{nm}^{(1)}$ and vice versa (2.43) and (2.44) can be represented in the following form, which may be more convenient for numerical simulation:

$$\sum_{v=|m|}^{\infty} (\delta_{nv} - U_{nmv}^{(j)}) B_{vm}^{(j)} = V_{nm}^{(j)}, \tag{2.46}$$

where

$$U_{nmv}^{(j)} = Q_n^{(j)} \sum_{l=|m|}^{\infty} Q_l^{(3-j)} K_{nml}^{(j)} K_{lmv}^{(3-j)}, \tag{2.47}$$

$$V_{nm}^{(j)} = Q_n^{(j)} \left(-A_{nm}^{(j)} + \sum_{l=|m|}^{\infty} Q_l^{(3-j)} K_{nml}^{(j)} A_{lm}^{(3-j)} \right). \tag{2.48}$$

Equation (2.31), which gives the force, is also reduced to

$$\begin{aligned} \boldsymbol{F}_j = \rho_0 \mathrm{Re} \sum_{n=0}^{\infty} \sum_{m=-n}^{n} D_n^{(j)} B_{nm}^{(j)} \Big\{ & 2\sqrt{(n+1)^2 - m^2}\, B_{(n+1)m}^{(j)*} \boldsymbol{e}_z \\ & + \Big[\sqrt{(n-m+1)(n-m+2)}\, B_{(n+1)(m-1)}^{(j)*} \\ & - \sqrt{(n+m+1)(n+m+2)}\, B_{(n+1)(m+1)}^{(j)*} \Big] \boldsymbol{e}_x \Big\}. \end{aligned} \tag{2.49}$$

Finally, the multipole coefficients $A_{nm}^{(j)}$ for a plane travelling wave can be written as

$$A_{nm}^{(1)} = 4\pi A \mathrm{i}^n Y_{nm}^*(\theta_I, 0), \quad A_{nm}^{(2)} = \exp(\mathrm{i}kL\cos\theta_I) A_{nm}^{(1)}, \tag{2.50}$$

and those for a plane standing wave are given by (2.39) with the proviso that $\varepsilon_I = 0$, $d_1 = d_o$ and $d_2 = d_o + L\cos\theta_I$.

2.6. *Forces on gas bubbles in the limit x_j, y_j, $R_j/r_{lj} \ll 1$; kr_{lj} is arbitrary*

In this subsection, (2.31) is applied to gas bubbles ($\rho_j \ll \rho_0$), assuming that the wavelength of sound in the host liquid, $\lambda = 2\pi/k$, the wavelength of sound inside the bubbles, $\lambda_j = 2\pi/k_j$, and the separation distances r_{lj} are much larger than the bubble radii R_j ($x_j, y_j, R_j/r_{lj} \ll 1$), while the ratio r_{lj}/λ is arbitrary. The ultimate goal of this subsection is to show that the new theory contains earlier results as a limiting case.

By using asymptotic expressions for the functions $j_n(x)$ and $h_n^{(1)}(x)$ in the limit $x \to 0$ (Abramowitz & Stegun 1972), from (2.19) and (2.21), with accuracy up to the leading terms in x_j and y_j, one finds

$$\alpha_0^{(j)} \approx \frac{\rho_j}{\rho_0} - \frac{2\sigma_j y_j^2}{3\rho_0 \omega^2 R_j^3}, \quad \alpha_1^{(j)} \approx \frac{\rho_j y_j}{3\rho_0}, \quad \alpha_2^{(j)} \approx \frac{y_j^2}{15}\left(\frac{\rho_j}{\rho_0} - \frac{2\omega_{2j}^2}{3\omega^2}\right), \tag{2.51}$$

$$\beta_0^{(j)} \approx -\frac{3\mathrm{i}}{x_j y_j^2}, \quad \beta_1^{(j)} \approx \frac{9\mathrm{i}}{x_j^2 y_j}, \quad \beta_2^{(j)} \approx \frac{225\mathrm{i}}{2x_j^3 y_j^2}\left(1 + \frac{2\omega_{2j}^2}{3\omega^2}\right)^{-1}, \tag{2.52}$$

where $\omega_{2j} = \sqrt{12\sigma_j/\rho_0 R_j^3}$ is the resonant frequency of the quadrupole surface mode of the jth bubble. Substituting (2.51) and (2.52) into (2.22), (2.24) and (2.32), one has

$$Q_0^{(j)} \approx \frac{\mathrm{i}x_j}{s_j}, \quad Q_1^{(j)} \approx \frac{x_j^3}{9}(3\mathrm{i} + x_j^3), \quad Q_2^{(j)} \approx \frac{\mathrm{i}x_j^5 \mu_j}{(1 - \omega_{2j}^2/\omega^2) + \mathrm{i}x_j^5 \mu_j}, \tag{2.53}$$

$$D_0^{(j)} \approx -\frac{\sqrt{3}}{4x_j^3}, \quad D_1^{(j)} \approx -\frac{1 - \omega_{2j}^2/\omega^2}{4\sqrt{15}x_j^5 \mu_j}, \tag{2.54}$$

where

$$s_j = 1 - \frac{\omega_j^2}{\omega^2} + \mathrm{i}x_j, \quad \mu_j = \frac{1}{45}\left(1 + \frac{2\omega_{2j}^2}{3\omega^2}\right), \tag{2.55}$$

and ω_j is the monopole resonance frequency of the jth bubble, defined as

$$\omega_j = \left(\frac{3\rho_j c_j^2}{\rho_0 R_j^2} - \frac{2\sigma_j}{\rho_0 R_j^3}\right)^{1/2}, \tag{2.56}$$

c_j being the speed of sound in the gas within the jth bubble. Finally, from (2.23), with the same accuracy, one obtains

$$B_{nm}^{(j)} \approx -Q_n^{(j)} A_{nm}^{(j)} - Q_n^{(j)} \sum_{\substack{l=1 \\ l \neq j}}^{N} K_{nm00}(k, \boldsymbol{r}_{lj}) B_{00}^{(l)}. \tag{2.57}$$

This equation shows that the order of the scattering coefficients is determined by the first term on the right-hand side, which is due to the direct impact of the incident field, whereas the second is a correction that is caused by the scattered field from the other bubbles.

Analysis of (2.53) and (2.57) allows us to make the following inferences about the order of the scattering coefficients:

$$\begin{gathered} B_{00}^{(j)} \sim x_j + O(x_j^2), \quad B_{1m}^{(j)} \sim x_j^3 + O(x_j^4), \\ B_{2m}^{(j)} \sim x_j^5 + O(x_j^6), \ldots, \quad B_{nm}^{(j)} \sim x_j^{2n+1} + O(x_j^{2n+2}). \end{gathered} \tag{2.58}$$

These equations, together with (2.54), allow us to estimate the order of the successive terms of the series (2.31):

$$D_0^{(j)} B_{00}^{(j)} B_{1m}^{(j)*} \sim x_j + O(x_j^2), \quad D_1^{(j)} B_{1m}^{(j)} B_{2m}^{(j)*} \sim x_j^3, \ldots, \quad D_n^{(j)} B_{nm}^{(j)} B_{n+1m}^{(j)*} \sim x_j^{2n+1}. \tag{2.59}$$

It immediately follows that the main contribution to the force comes from the zero

term and results in

$$\boldsymbol{F}_j = -\frac{\sqrt{3}\rho_0}{\sqrt{8}x_j^3}\mathrm{Re}\{\sqrt{2}B_{00}^{(j)}B_{10}^{(j)*}\boldsymbol{e}_z + B_{00}^{(j)}B_{1-1}^{(j)*}(\boldsymbol{e}_x + \mathrm{i}\boldsymbol{e}_y) - B_{00}^{(j)}B_{11}^{(j)*}(\boldsymbol{e}_x - \mathrm{i}\boldsymbol{e}_y)\}. \tag{2.60}$$

The scattering coefficients appearing here are given by

$$B_{00}^{(j)} = -\frac{x_j}{s_j}\left[\mathrm{i}A_{00}^{(j)} + \sum_{\substack{l=1\\ l\neq j}}^{N}\frac{x_l}{s_l}h_0^{(1)}(kr_{lj})A_{00}^{(l)}\right], \tag{2.61}$$

$$B_{1m}^{(j)} = -\frac{x_j^3}{3}\left[\mathrm{i}A_{1m}^{(j)} - \sqrt{4\pi}\sum_{\substack{l=1\\ l\neq j}}^{N}\frac{x_l}{s_l}h_1^{(1)}(kr_{lj})Y_{1m}^*(\theta_{lj},\varepsilon_{lj})A_{00}^{(l)}\right], \quad m = -1, 0, 1. \tag{2.62}$$

The first (leading) terms in brackets on the right-hand sides of (2.61) and (2.62) provide the primary radiation forces. It is easy to verify, substituting (2.36) and (2.39) for $A_{nm}^{(j)}$, that when only these terms are retained, formula (2.60) gives the well-known expressions for the primary radiation force acting on the jth bubble in, respectively, a plane travelling wave and a plane standing wave:

$$\boldsymbol{F}_{Pj}^{(tr)} = 2\pi\rho_0|A|^2x_j^2|s_j|^{-2}\boldsymbol{k}/k, \tag{2.63}$$

$$\boldsymbol{F}_{Pj}^{(st)} = \pi\rho_0|A|^2x_j|s_j|^{-2}(1-\omega_j^2/\omega^2)\sin(2kd_j)\boldsymbol{k}/k. \tag{2.64}$$

The secondary radiation forces, which are our prime interest, are produced by the cross-products of the first and second terms in brackets. The limit analogous to that considered here was first investigated by Doinikov & Zavtrak (1997) for the case of two-bubble interaction. In order to show that the new theory recovers their results, we also apply (2.60)–(2.62) to the case of two bubbles. Assuming that the two bubbles are located as shown in figure 2, (2.61) and (2.62) take the form

$$B_{00}^{(j)} = -\frac{x_j}{s_j}[\mathrm{i}A_{00}^{(j)} + x_{3-j}h_0^{(1)}(kL)A_{00}^{(3-j)}/s_{3-j}], \quad j = 1, 2, \tag{2.65}$$

$$B_{1m}^{(j)} = -\tfrac{1}{3}x_j^3[\mathrm{i}A_{1m}^{(j)} - (1-|m|)\sqrt{3}(-1)^jx_{3-j}h_1^{(1)}(kL)A_{00}^{(3-j)}/s_{3-j}], \quad m = -1, 0, 1. \tag{2.66}$$

Substituting these equations into (2.60) and retaining only the cross-terms, one obtains the secondary force as

$$\boldsymbol{F}_{Sj} = -\frac{1}{2}\rho_0x_1x_2\mathrm{Im}\left\{\frac{(-1)^jh_1^{(1)*}(kL)}{s_js_{3-j}^*}A_{00}^{(j)}A_{00}^{(3-j)*}\boldsymbol{e}_z + \frac{h_0^{(1)}(kL)}{\sqrt{6}\,s_js_{3-j}}A_{00}^{(3-j)}[\sqrt{2}A_{10}^{(j)*}\boldsymbol{e}_z + (A_{1-1}^{(j)*} - A_{11}^{(j)*})\boldsymbol{e}_x]\right\}, \quad j = 1, 2. \tag{2.67}$$

For a plane travelling wave and plane standing wave, (2.67) gives, respectively,

$$\boldsymbol{F}_{Sj}^{(tr)} = \frac{2\pi\rho_0|A|^2R_1R_2}{|s_1|^2|s_2|^2L^2}\,\mathrm{Im}\{(-1)^{j+1}(\mathrm{i}-kL)\boldsymbol{e}^{-\mathrm{i}\chi_j}s_j^*s_{3-j}\boldsymbol{e}_z + \mathrm{e}^{\mathrm{i}\chi_j}(s_1s_2)^*L\boldsymbol{k}\}, \tag{2.68}$$

$$\boldsymbol{F}_{Sj}^{(st)} = \frac{2\pi\rho_0|A|^2R_1R_2}{|s_1|^2|s_2|^2L^2}\,\mathrm{Re}\{(-1)^{j+1}(1+\mathrm{i}kL)\mathrm{e}^{-\mathrm{i}kL}s_j^*s_{3-j}\cos(kd_1)\cos(kd_2)\boldsymbol{e}_z$$
$$-\mathrm{e}^{\mathrm{i}kL}(s_1s_2)^*\sin(kd_j)\cos(kd_{3-j})L\boldsymbol{k}\}, \tag{2.69}$$

where $\chi_j = kL[1-(-1)^j\cos\theta_I]$. Comparison of (2.68) and (2.69) with the corresponding equations obtained in Doinikov & Zavtrak (1997) shows that they are in perfect agreement. Furthermore, in the limit $k \to 0$ both (2.68) and (2.69) reduce to

$$\boldsymbol{F}_{Sj}^{(tr)} = \frac{2\pi\rho_0|A|^2R_1R_2(-1)^{j+1}\boldsymbol{e}_z}{(1-\omega_1^2/\omega^2)(1-\omega_2^2/\omega^2)L^2}, \tag{2.70}$$

which is simply the classical Bjerknes formula for the radiation interaction force between two gas bubbles in an incompressible ideal fluid (Crum 1975).

3. Numerical results

Numerical simulations have been made for two air bubbles in water. To perform a more adequate comparison with the Bjerknes theory, the case was first run where the bubbles were subject to a plane travelling wave propagating from left to right along their centreline. Some representative results are plotted in figures 3–5 that show the normalized (divided by $|A|^2$) interaction force on the left-hand bubble versus the dimensionless separation distance defined as $D = L/(R_1 + R_2)$. Shown dotted are predictions of the Bjerknes theory, equation (2.70). The solid curves present the force that is obtained from (2.49) minus the primary radiation force. The latter is calculated from (2.63). It was found that in all the cases investigated the series (2.49) converged monotonically and fast. Therefore five first terms of (2.49) are sufficient to calculate the force to a very good accuracy. For the cases shown in figures 3 and 5, the relative error due to the truncation of (2.49) was found not to exceed 0.02%. In the case shown in figure 4, where the second bubble is very close to resonance, the error is larger, up to 0.66% at small separations.

Figure 3 illustrates the behaviour of two bubbles of equal size that are driven above their monopole resonance frequency. It can be seen that the Bjerknes theory is only valid for intermediate separation distances. For small separations, figure 3(*a*), it greatly overestimates the force because of ignoring multiple re-scattering of sound between the bubbles and their shape modes. For large separations, figure 3(*b*), the Bjerknes theory predicts only a rapid decrease of the force in magnitude. What actually happens is that the sign of the force oscillates, which is a consequence of the finite compressibility of the host liquid. Note also that the first sign reversal occurs at the separation distance $D \approx 33$, which is much smaller than the value $D = 150$ corresponding to the wavelength of sound in the host liquid. To gain an insight into why this happens, we can apply equation (2.68). We are able to do this since the case we examine here corresponds to the limit investigated in § 2.6. Then, setting $\boldsymbol{k} \| \boldsymbol{e}_z$ and neglecting radiation losses, one obtains from (2.68) the secondary force on the left-hand bubble (bubble 1) as

$$\boldsymbol{F}_{S1}^{(tr)} = \frac{2\pi\rho_0|A|^2x_1x_2}{(1-\omega_1^2/\omega^2)(1-\omega_2^2/\omega^2)}G(kL)\boldsymbol{e}_z \tag{3.1}$$

with $G(kL) = (kL)^{-2}\cos(2kL) + 2(kL)^{-1}\sin(2kL)$. According to (2.50), the phase shift between the primary (induced by the forcing) oscillations of the bubbles is given by kL. This means that the bubbles begin to oscillate out of phase at $L = 0.25\lambda$. At first sight one could expect that the interaction force between them should also change its

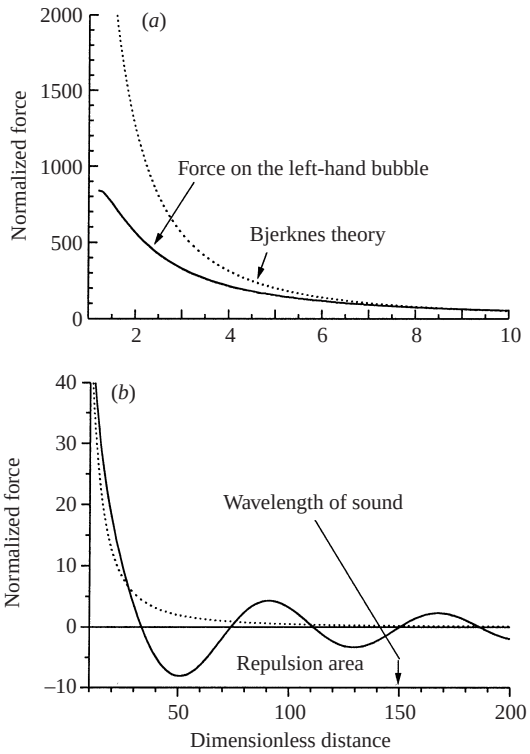

FIGURE 3. Interaction force between two bubbles of equal size ($R_1 = R_2 = 50\,\mu$m), driven above resonance, as a function of the separation distance. The forcing is a plane travelling wave with the frequency $f = 100$ kHz, propagating along the centreline of the bubbles from the left to the right.

sign at the same value of L. However, the force is a nonlinear (quadratic) effect that results from the interaction between the combined oscillation of the bubble, which is induced by both the forcing and the scattered wave from the other bubble, and the overall action on it, which also includes both the forcing and the scattered field of the other bubble. In the case of a compressible fluid, the structure of all the constituents of this process is fairly intricate. As a consequence, the dependence of the force on L is determined by the rather complicated function $G(kL)$. Analysis of this latter shows that it first changes sign at $L \approx 0.22\lambda$, which is in agreement with what is seen in figures 3–5. Recall that the figures were obtained numerically on the basis of the exact equation (2.49), while (3.1) is an asymptotic formula that was derived analytically in the limit x_j, y_j, $R_j/r_{lj} \ll 1$. Therefore the good agreement between them can be regarded as one more verification of the new extended theory.

Figure 4 gives an idea of the interaction between two bubbles of unequal size that are driven in such a way that the monopole resonance frequency of the smaller bubble is not much below the driving frequency. It can be seen that in this case the deviation from the Bjerknes theory is even more substantial. At large separations, a more profound oscillation of the force is detected. At small separations, the force also changes from attraction to repulsion and thus keeps the bubbles from coalescing, which should have been expected according to the Bjerknes theory. Finally figure 5 exemplifies the interaction between two bubbles driven below resonance. For large separations, the oscillation of the sign of the force due to the liquid compressibility is again observed, although it is now much softer than in the two preceding cases. At

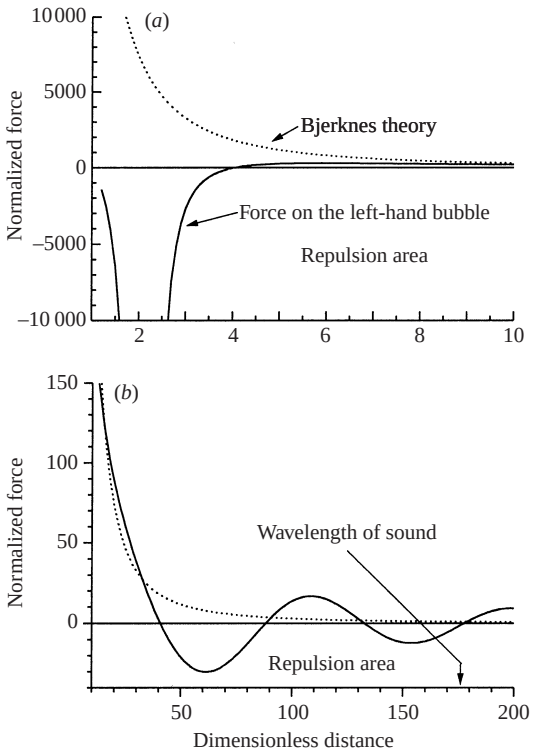

FIGURE 4. Interaction force between two bubbles of unequal size ($R_1 = 50\,\mu m$, $R_2 = 35\,\mu m$) driven above resonance. The forcing is as in figure 3.

small separations, the force is found to be much larger than is given by the Bjerknes theory. This should lead to a much faster coalescence of such bubbles.

Let us now turn to more realistic cases where the wavevector does not coincide with the centreline of the bubbles. The following figures present trajectories of the 'slow' (time-averaged) translational motion of interacting bubble pairs, assuming that the acoustic radiation force, given by (2.49), is balanced by the viscous drag force, given by (Landau & Lifshitz 1959)

$$\boldsymbol{F}_{vj} = -4\pi\eta R_j \boldsymbol{U}_j, \tag{3.2}$$

where η is the liquid viscosity and $\boldsymbol{U}_j$ is the time-averaged translational velocity of the jth bubble. The inertial, buoyant and other forces are neglected for the sake of simplicity because, first, the purpose of this study is to give an indication of the effects of liquid compressibility on acoustic interparticle forces rather than accurate modelling of bubble motions with the entire variety of natural processes, and second, in many cases of interest the above forces are really dominated by the viscous drag.

As a compromise between speed of simulations and their accuracy, the radiation force was calculated up to three first terms of (2.49). This is a satisfactory approximation since in all test cases the magnitude of the fourth (neglected) term of (2.49) with respect to that of the first (dominant) term was found not to exceed 4%. In some situations, however, the fourth term can play a part. In particular, in the cases shown in figure 6(*a–c*), when the interaction force reverses at small distances, the first three terms of (2.49) tend to cancel one another and therefore the contribution of the

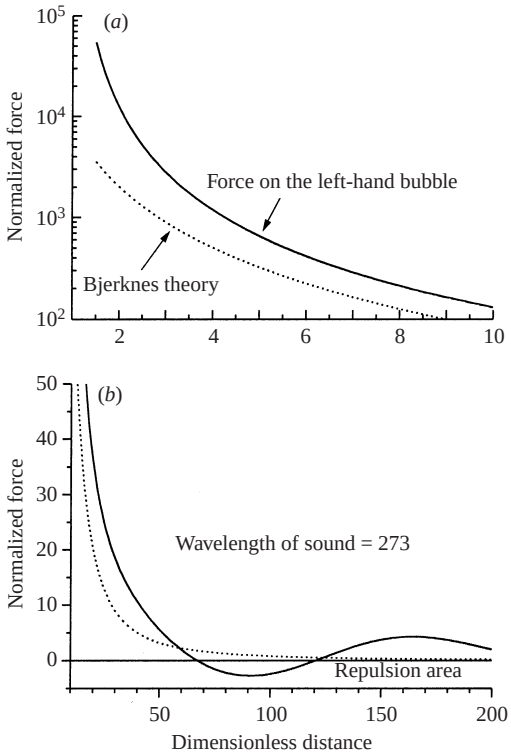

FIGURE 5. Interaction force between two bubbles of unequal size ($R_1 = 30\,\mu$m, $R_2 = 25\,\mu$m) driven below resonance. The forcing is as in figure 3.

fourth term to the net force may be relatively large, although this changes nothing in a qualitative sense. In such situations, the force was calculated up to the fourth term.

Figure 6 gives an overview of bubble trajectories in a plane travelling wave incident at various angles θ_I on bubble pairs of various radii R_1 and R_2. The sound wave first reaches the left-hand bubble, the driving frequency f is 130 kHz, and the acoustic pressure amplitude is $0.1\,P_0$. The x- and y-axes of figure 6 are marked in terms of dimensionless units of length that are defined as $D = d/(R_1 + R_2)$, where d is dimensional distance. The arrows next to the curves indicate the direction of bubble motion. Shown dashed are predictions of the Bjerknes theory, which are obtained from (2.63) and (2.70). In figure 6(a), $\theta_I = \pi/3$, the temporal interval of computation $T = 100$ a.c. (where a.c. means 'acoustic cycles'), and R_1 and R_2 are equal to 50 μm and 30 μm, respectively, which corresponds to the resonant frequencies $f_1 = 66$ kHz and $f_2 = 110.9$ kHz. Thus, both bubbles are driven above resonance. Therefore initially they are attracted to each other, slowly moving in the direction of wave propagation. According to the Bjerknes theory, the bubbles come into contact (and then probably coalesce) within the interval $T_c = 19$ a.c. The extended theory shows, however, that the interaction force becomes repulsive at small separations, as in figure 4, and the bubbles stop approaching. Figure 6(b) shows the same bubble pair but at $\theta_I = \pi/6$ and over $T = 500$ a.c. It is seen that the change of the angle of incidence of sound noticeably changes the pattern of motion. The left-hand bubble now moves much faster than the right-hand one. This is likely to be associated with the y-component of

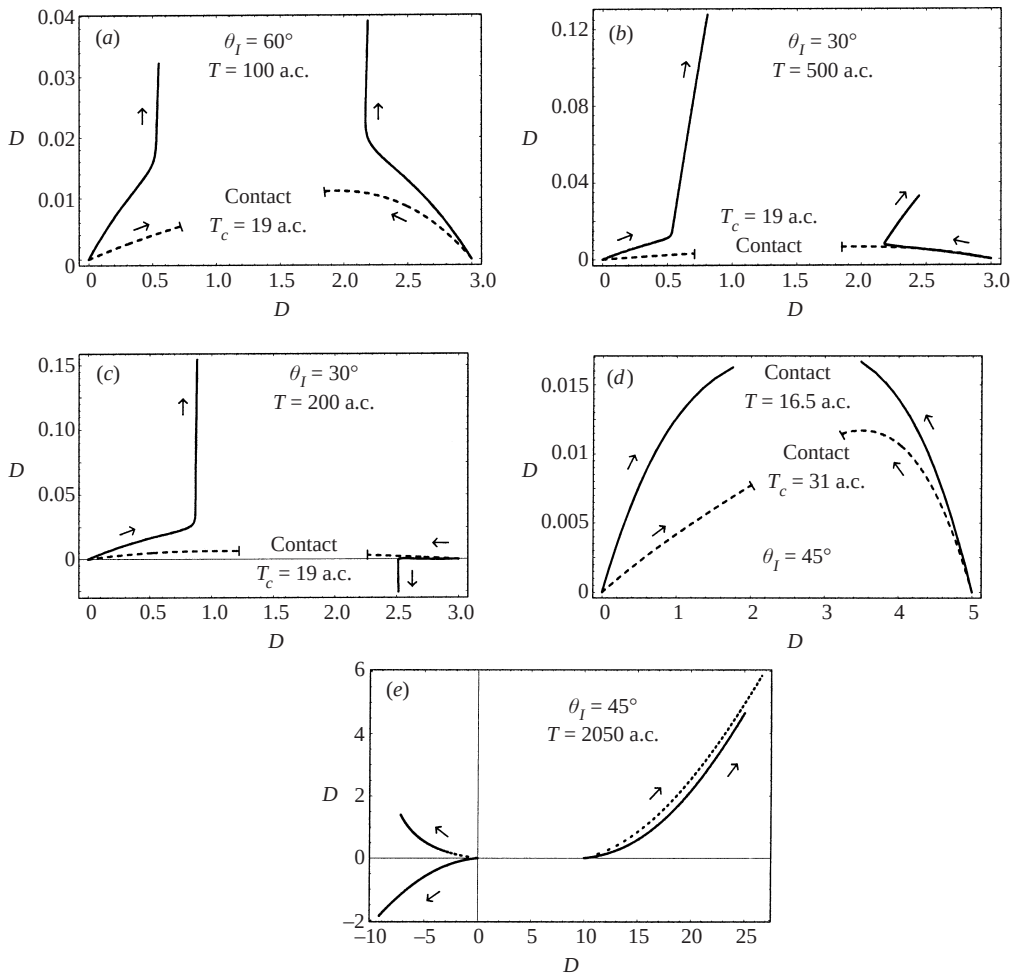

FIGURE 6. Trajectories of the time-averaged motion of two interacting bubbles in a plane travelling wave; the x- and y-axes are marked in terms of dimensionless units of length, the driving frequency $f = 130\,\text{kHz}$, the acoustic pressure amplitude is $0.1P_0$: (*a*) $\theta_I = \pi/3$, $R_1 = 50\,\mu\text{m}$ ($f_1 = 66\,\text{kHz}$), $R_2 = 30\,\mu\text{m}$, ($f_2 = 110.9\,\text{kHz}$; (*b*) $\theta_I = \pi/6$, $R_1 = 50\,\mu\text{m}$, $R_2 = 30\,\mu\text{m}$; (*c*) $\theta_I = \pi/6$, $R_1 = 30\,\mu\text{m}$, $R_2 = 50\,\mu\text{m}$; (*d*) $\theta_I = \pi/4$, $R_1 = 20\,\mu\text{m}$ ($f_1 = 167.8\,\text{kHz}$), $R_2 = 22\,\mu\text{m}$ ($f_2 = 152.2\,\text{kHz}$); (*e*) $\theta_I = \pi/4$, $R_1 = 30\,\mu\text{m}$, $R_2 = 24\,\mu\text{m}$ ($f_2 = 139.2\,\text{kHz}$).

the interaction force, which at the given value of θ_I is increased and added favourably to the primary radiation force on the left-hand bubble.

Note that physically it would be more correct to talk about the components of the interaction force along the centreline of the bubbles and along the wavevector of the imposed field, because it is clear that it is along those two natural spatial directions that the actual components of the interaction force lie. However, we use the Cartesian coordinates and therefore it is more convenient here to refer to components along the x- and y-axes.

Parameters in figure 6(*c*) are the same as in figure 6(*b*), except that the bubbles swap places. In other words, the situation is as if the sound field in figure 6(*b*) were incident from the right. This again leads to a different pattern of motion and we can see another manifestation of the y-component of the interaction force. This time it

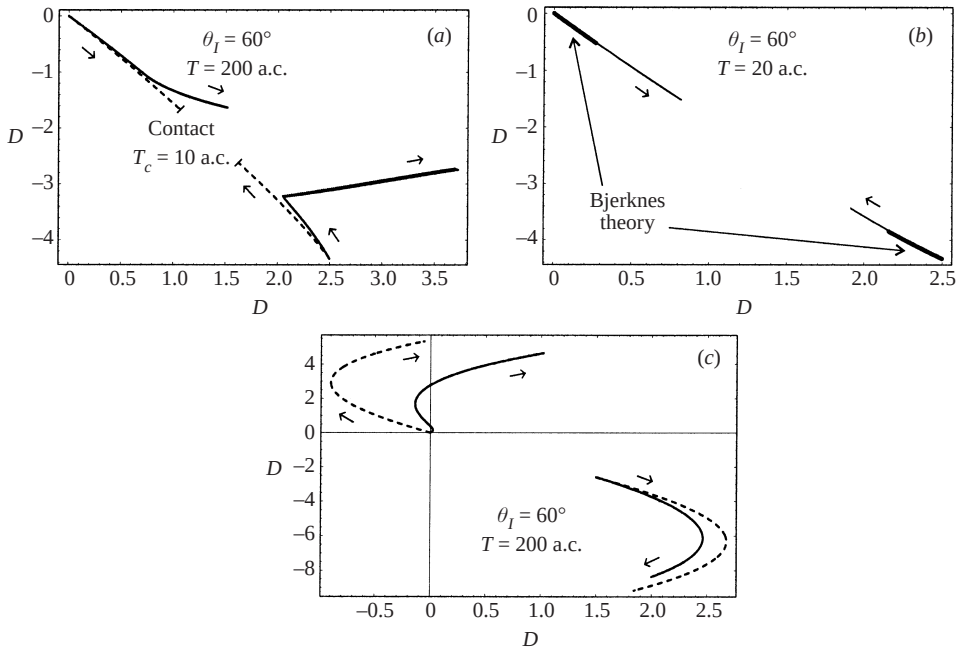

FIGURE 7. Trajectories of the time-averaged motion of two interacting bubbles in a plane standing wave; the x- and y-axes are marked in terms of dimensionless units of length, the driving frequency $f = 100\,\mathrm{kHz}$, the acoustic pressure amplitude is $0.1P_0$, the angle of sound incidence $\theta_I = \pi/3$: (*a*) $D_0 = 10$, $R_1 = 38\,\mu\mathrm{m}$ ($f_1 = 87.2\,\mathrm{kHz}$), $R_2 = 37\,\mu\mathrm{m}$ ($f_2 = 89.6\,\mathrm{kHz}$); (*b*) $D_0 = 5$, $R_1 = 25\,\mu\mathrm{m}$ ($f_1 = 133.5\,\mathrm{kHz}$), $R_2 = 27\,\mu\mathrm{m}$ ($f_2 = 123.4\,\mathrm{kHz}$); (*c*) $D_0 = 10$, $R_1 = 37\,\mu\mathrm{m}$ ($f_1 = 89.6\,\mathrm{kHz}$), $R_2 = 30\,\mu\mathrm{m}$ ($f_2 = 110.9\,\mathrm{kHz}$).

counteracts the primary radiation force on the right-hand bubble and causes it to move against the sound wave. In figure 6(*d*), $\theta_I = \pi/4$, $R_1 = 20\,\mu\mathrm{m}$ ($f_1 = 167.8\,\mathrm{kHz}$) and $R_2 = 22\,\mu\mathrm{m}$ ($f_2 = 152.2\,\mathrm{kHz}$). Thus, this figure illustrates the behaviour of two bubbles that are driven below resonance. They are seen to experience strong mutual attraction and come into contact very fast, within 16.5 a.c. The Bjerknes theory also predicts the collision of the bubbles, but within a longer interval of 31 a.c. Finally, figure 6(*e*) shows the motion of two bubbles one of which, the left-hand bubble ($R_1 = 30\,\mu\mathrm{m}$, $f_1 = 110.9\,\mathrm{kHz}$), is driven above resonance, while the other, the right-hand bubble ($R_2 = 24\,\mu\mathrm{m}$, $f_2 = 139.2\,\mathrm{kHz}$), below resonance. The bubbles are repelled along their centreline, as the Bjerknes theory predicts. At the same time, however, due to the non-zero angle of incidence of sound ($\theta_I = \pi/4$), we again observe an action of the transversal component of the interaction force. It predominates over the primary radiation force on the left-hand bubble and thus makes it move in the left lower instead of upper quadrant of the coordinate system.

Figure 7 shows the motion of the bubbles in a plane standing wave. The nearest velocity node plane is on the left, the wave front is parallel to the y-axis, the wavevector lies along the x-axis, the frequency is 100 kHz and the acoustic pressure amplitude is $0.1\,P_0$. As in figure 6, the coordinate axes are marked in terms of a dimensionless unit of length and their origin is at the initial position of the equilibrium centre of the left-hand bubble, which is at a distance D_0 (in dimensionless units) from the velocity node plane. The dashed curves correspond to the Bjerknes theory, equations (2.64)

and (2.70), except for figure 7(*b*) where the predictions of the Bjerknes theory are shown by thick lines.

In figure 7(*a*), both bubbles are driven above resonance. The primary radiation force on bubbles of this sort is directed away from velocity nodes. However, the interaction force is seen to overcome the primary force and causes the right-hand bubble to move at first towards the left-hand one, against the wavevector. The Bjerknes theory predicts the contact of the bubbles within the interval $T_c = 10$ a.c. According to the extended theory, at a smaller spacing the interaction force becomes repulsive and the right-hand bubble makes a sharp right turn. Closer inspection also reveals that the bubbles' trajectories are formed by small reciprocal motions as the force is alternately attractive and repulsive. Figure 7(*b*) exemplifies the motion of the bubbles when they are driven below resonance. Both theories predict collision and coalescence, but the Bjerknes theory (thick lines) underestimates considerably the rate of approach. Figure 7(*c*) demonstrates a very interesting pattern of motion. In this figure, the left-hand bubble is driven above resonance, and the right-hand one, below resonance. Therefore the left-hand bubble is subject to the primary force directed away from velocity nodes, and the right-hand one, towards velocity nodes, while the interaction force acting along their centreline is repulsive. It is these opposite forces that make the bubbles take such a curious path. Again, as in figure 7(*b*), although the predictions of the two theories agree qualitatively, there is a considerable quantitative discrepancy. This time the Bjerknes theory overestimates the repulsive interaction force.

4. Conclusion

An analytical expression has been derived for the time-averaged radiation interparticle force due to an acoustic wave field, assuming the media outside and inside particles to be ideal compressible fluids, allowing for multiple re-scattering of sound between the particles and their shape distortions, and imposing no restrictions on the wavelength of sound, the number of the particles, their radii and the separation distances between them. To test capabilities of the new theory, numerical calculations have been carried out for two air bubbles in water for two types of forcing: a plane travelling wave and a plane standing wave. Comparison has been made with predictions of the Bjerknes theory. It has been shown that in the general case the behaviour of the interparticle forces is far more complicated than is predicted by the Bjerknes theory. It is expected that the new theory will make possible a more correct modelling of collective behaviour of bubbles and drops in acoustic fields.

This research was supported by the European Commission under contract IC15-CT98-0141.

Appendix. Integrals I_1, I_2, I_3

The above integrals, defined by (2.27)–(2.29), are calculated by means of putting them in the form of a sum of integrals of the following form:

$$\int_0^{2\pi} \mathrm{d}\varepsilon \int_0^{\pi} \mathrm{d}\theta \sin\theta \, Y^*_{nm}(\theta,\varepsilon) Y_{n'm'}(\theta,\varepsilon) = \delta_{nn'}\delta_{mm'}, \tag{A 1}$$

where δ_{nm} is the Kronecker delta. This equation is known as the orthogonality condition of spherical harmonics.

A.1. *Calculation of* $\boldsymbol{I}_1(n,m,n',m')$

The integral $\boldsymbol{I}_1$ is easily made into a sum of integrals (A 1), using the recurrence formulae for spherical harmonics (Varshalovich *et al.* 1975):

$$\cos\theta\, Y_{nm}(\theta,\varepsilon) = \gamma_{n+1m} Y_{n+1m}(\theta,\varepsilon) + \gamma_{nm} Y_{n-1m}(\theta,\varepsilon), \tag{A 2}$$

$$\sin\theta\, Y_{nm}(\theta,\varepsilon)\mathrm{e}^{\mathrm{i}\varepsilon} = \mu_{n(-m)} Y_{n-m+1}(\theta,\varepsilon) - \mu_{n+1m+1} Y_{n+1m+1}(\theta,\varepsilon), \tag{A 3}$$

$$\sin\theta\, Y_{nm}(\theta,\varepsilon)\mathrm{e}^{-\mathrm{i}\varepsilon} = \mu_{n+11-m} Y_{n+1m-1}(\theta,\varepsilon) - \mu_{nm} Y_{n-1m-1}(\theta,\varepsilon), \tag{A 4}$$

where

$$\gamma_{nm} = \sqrt{\frac{n^2-m^2}{(2n-1)(2n+1)}} \quad \text{and} \quad \mu_{nm} = \sqrt{\frac{(n+m-1)(n+m)}{(2n-1)(2n+1)}}. \tag{A 5}$$

The final result is given by

$$\boldsymbol{I}_1(n,m,n',m') = I_{1x}\boldsymbol{e}_x + I_{1y}\boldsymbol{e}_y + I_{1z}\boldsymbol{e}_z, \tag{A 6}$$

$$\begin{aligned} I_{1x} = \tfrac{1}{2}(&\mu_{n+11-m}\delta_{n+1n'}\delta_{m-1m'} + \mu_{n(-m)}\delta_{n-1n'}\delta_{m+1m'} \\ &-\mu_{nm}\delta_{n-1n'}\delta_{m-1m'} - \mu_{n+1m+1}\delta_{n+1n'}\delta_{m+1m'}), \end{aligned} \tag{A 7}$$

$$\begin{aligned} I_{1y} = \tfrac{1}{2}\mathrm{i}(&\mu_{n+1m+1}\delta_{n+1n'}\delta_{m+1m'} - \mu_{n(-m)}\delta_{n-1n'}\delta_{m+1m'} \\ &-\mu_{nm}\delta_{n-1n'}\delta_{m-1m'} + \mu_{n+11-m}\delta_{n+1n'}\delta_{m-1m'}), \end{aligned} \tag{A 8}$$

$$I_{1z} = (\gamma_{n+1m}\delta_{n+1n'} + \gamma_{nm}\delta_{n-1n'})\delta_{mm'}. \tag{A 9}$$

A.2. *Calculation of* $\boldsymbol{I}_2(n,m,n',m')$

To reduce this integral to a sum of integrals (A 1), the following equations are applied (Varshalovich *et al.* 1975):

$$\nabla Y_{nm}(\theta,\varepsilon) = \boldsymbol{e}_0\nabla_0 Y_{nm}(\theta,\varepsilon) - \boldsymbol{e}_{+1}\nabla_{-1} Y_{nm}(\theta,\varepsilon) - \boldsymbol{e}_{-1}\nabla_{+1} Y_{nm}(\theta,\varepsilon), \tag{A 10}$$

$$\nabla_0 Y_{nm}(\theta,\varepsilon) = (n+1)\gamma_{nm} r^{-1} Y_{n-1m}(\theta,\varepsilon) - n\gamma_{n+1m} r^{-1} Y_{n+1m}(\theta,\varepsilon), \tag{A 11}$$

$$\nabla_{+1} Y_{nm}(\theta,\varepsilon) = -\frac{n\mu_{n+1m+1}}{r\sqrt{2}} Y_{n+1m+1}(\theta,\varepsilon) - \frac{(n+1)\mu_{n(-m)}}{r\sqrt{2}} Y_{n-1m+1}(\theta,\varepsilon), \tag{A 12}$$

$$\nabla_{-1} Y_{nm}(\theta,\varepsilon) = -\frac{n\mu_{n+11-m}}{r\sqrt{2}} Y_{n+1m-1}(\theta,\varepsilon) - \frac{(n+1)\mu_{nm}}{r\sqrt{2}} Y_{n-1m-1}(\theta,\varepsilon), \tag{A 13}$$

where

$$\boldsymbol{e}_0 = \boldsymbol{e}_z, \quad \boldsymbol{e}_{+1} = -\frac{1}{\sqrt{2}}(\boldsymbol{e}_x + \mathrm{i}\boldsymbol{e}_y), \quad \boldsymbol{e}_{-1} = \frac{1}{\sqrt{2}}(\boldsymbol{e}_x - \mathrm{i}\boldsymbol{e}_y).$$

The resulting expression is as follows:

$$\boldsymbol{I}_2(n,m,n',m') = I_{2x}\boldsymbol{e}_x + I_{2y}\boldsymbol{e}_y + I_{2z}\boldsymbol{e}_z, \tag{A 14}$$

$$\begin{aligned} I_{2x} = \tfrac{1}{2}(&n\mu_{n+1m+1}\delta_{n+1n'}\delta_{m+1m'} + (n+1)\mu_{n(-m)}\delta_{n-1n'}\delta_{m+1m'} \\ &-n\mu_{n+11-m}\delta_{n+1n'}\delta_{m-1m'} - (n+1)\mu_{nm}\delta_{n-1n'}\delta_{m-1m'}), \end{aligned} \tag{A 15}$$

$$\begin{aligned} I_{2y} = -\tfrac{1}{2}\mathrm{i}(&n\mu_{n+1m+1}\delta_{n+1n'}\delta_{m+1m'} + (n+1)\mu_{n(-m)}\delta_{n-1n'}\delta_{m+1m'} \\ &+n\mu_{n+11-m}\delta_{n+1n'}\delta_{m-1m'} + (n+1)\mu_{nm}\delta_{n-1n'}\delta_{m-1m'}), \end{aligned} \tag{A 16}$$

$$I_{2z} = [(n+1)\gamma_{nm}\delta_{n-1n'} - n\gamma_{n+1m}\delta_{n+1n'}]\delta_{mm'}. \tag{A 17}$$

A.3. *Calculation of* $\boldsymbol{I}_3(n,m,n',m')$

This, most cumbersome integral is obtained using jointly (A 2)–(A 4) and (A 10)–(A 13):

$$\boldsymbol{I}_3(n,m,n',m') = I_{3x}\boldsymbol{e}_x + I_{3y}\boldsymbol{e}_y + I_{3z}\boldsymbol{e}_z, \tag{A 18}$$

$$\begin{aligned} I_{3x} = \tfrac{1}{2}[&n(n+2)\mu_{n+11-m}\delta_{n+1n'}\delta_{m-1m'} + (n^2-1)\mu_{n(-m)}\delta_{nn'+1}\delta_{mm'-1} \\ &-n(n+2)\mu_{n+1m+1}\delta_{n+1n'}\delta_{m+1m'} - (n^2-1)\mu_{nm}\delta_{nn'+1}\delta_{mm'+1}], \end{aligned} \tag{A 19}$$

$$\begin{aligned} I_{3y} = \tfrac{1}{2}\mathrm{i}[&n(n+2)\mu_{n+1m+1}\delta_{n+1n'}\delta_{m+1m'} - (n^2-1)\mu_{nm}\delta_{nn'+1}\delta_{mm'+1} \\ &+n(n+2)\mu_{n+11-m}\delta_{n+1n'}\delta_{m-1m'} - (n^2-1)\mu_{n(-m)}\delta_{nn'+1}\delta_{mm'-1}], \end{aligned} \tag{A 20}$$

$$I_{3z} = [n(n+2)\gamma_{n+1m}\delta_{n+1n'} + (n^2-1)\gamma_{nm}\delta_{nn'+1}]\delta_{mm'}. \tag{A 21}$$

REFERENCES

Abramowitz, M. & Stegun, I. A. 1972 *Handbook of Mathematical Functions*. Dover.

Alekseev, V. N. 1983 Force produced by the acoustic radiation pressure on a sphere. *Sov. Phys. Acoust.* **29**, 77–81.

Brennen, C. E. 1995 *Cavitation and Bubble Dynamics*. Oxford University Press.

Crum, L. A. 1975 Bjerknes forces on bubbles in a stationary sound field. *J. Acoust. Soc. Am.* **57**, 1363–1370.

Doinikov, A. A. 1996 Mutual interaction between a bubble and a drop in a sound field. *J. Acoust. Soc. Am.* **99**, 3373–3379.

Doinikov, A. A. & Zavtrak, S. T. 1995 On the mutual interaction of two gas bubbles in a sound field. *Phys. Fluids* **7**, 1923–1930.

Doinikov, A. A. & Zavtrak, S. T. 1996 Interaction force between a bubble and a solid particle in a sound field. *Ultrasonics* **34**, 807–815.

Doinikov, A. A. & Zavtrak, S. T. 1997 Radiation forces between two bubbles in a compressible liquid. *J. Acoust. Soc. Am.* **102**, 1424–1431.

Embleton, T. F. W. 1962 Mutual interaction between two spheres in a plane sound field. *J. Acoust. Soc. Am.* **34**, 1714–1720.

Kobelev, Yu. A., Ostrovskii, L. A. & Sutin, A. M. 1979 Effect of self-clearing for acoustic waves in a liquid with gas bubbles. *Pis'ma Zh. Eksp. Teor. Fiz.* **30**, 423–425.

Koc, S. & Chew, W. C. 1998 Calculation of acoustical scattering from a cluster of scatterers. *J. Acoust. Soc. Am.* **103**, 721–734.

König, W. 1891 Hydrodynamisch-akustische Untersuchungen. *Ann. Phys.* **42**, 549–563.

Lamb, H. 1945 *Hydrodynamics*. Dover

Landau, L. D. & Lifshitz, E. M. 1959 *Fluid Mechanics*. Pergamon.

Mednikov, E. P. 1965 *Acoustic Coagulation and Precipitation of Aerosols*. Consultants Bureau, New York.

Mettin, R., Akhatov, I., Parlitz, U., Ohl, C. D. & Lauterborn, W. 1997 Bjerknes forces between small cavitation bubbles in a strong acoustic field. *Phys. Rev.* E **56**, 2924–2931.

Pelekasis, N. A. & Tsamopoulos, J. A. 1993*a* Bjerknes forces between two bubbles. Part 1. Response to a step change in pressure. *J. Fluid Mech.* **254**, 467–499.

Pelekasis, N. A. & Tsamopoulos, J. A. 1993*b* Bjerknes forces between two bubbles. Part 2. Response to an oscillatory pressure field. *J. Fluid Mech.* **254**, 501–527.

Prosperetti, A. 1977 Viscous effects on perturbed spherical flows. *Q. Appl. Maths* **34**, 339–352.

Rozenberg, L. D. (Ed.) 1973 *Physical Principles of Ultrasonic Technology*. Plenum.

Varshalovich, D. A., Moskalev, A. N. & Khersonskii, V. K. 1975 *Quantum Theory of Angular Momentum*. Nauka.

Weiser, M. A. H. & Apfel, R. E. 1984 Interparticle forces on red cells in a standing wave field. *Acustica* **56**, 114–119.

Zabolotskaya, E. A. 1984 Interaction of gas bubbles in a sound wave field. *Sov. Phys. Acoust*. **30**, 365–368.

Zheng, X. & Apfel, R. E. 1995 Acoustic interaction forces between two fluid spheres in an acoustic field. *J. Acoust. Soc. Am.* **97**, 2218–2226.